Design, Synthesis, and Evaluation of Pyrazole-Isoxazole Hybrids as Dual-Action Agents Against Biofilm-Forming Drug-Resistant Bacteria

Meena Kumari

Department of Chemistry, Kalinga University, Naya Raipur, Chattisgarh, India

**Author for correspondence: nikiisheoran@gmail.com*

ABSTRACT

The increasing rates of multidrug-resistant (MDR) bacterial infections with the complication of biofilm formation can pose a significant threat to global public health. The present work has involved rational design, synthesis and overall antimicrobial assessment of new pyrazole-isoxazole hybrid scaffolds which target non-adherent as well as adherent bacterial groups. compounds, N'-[(1-(4-chlorophenyl)-1H-pyrazol-4-yl)methylidene]-3-phenylisoxazole-5-carbohydrazide (H1) and N'-[(1-(4-methoxyphenyl)-1H-pyrazol-4-yl)methylidene]-3-phenylisoxazole-5-carbohydrazide (H2), were synthesized via acid-catalyzed condensation of substituted pyrazole-4-carbaldehydes with 3-phenylisoxazole-5-carbohydrazide, achieving yields of 82-85%. The structural elucidation was done using the ^{1}H-NMR, FT-IR, ESI-MS. *In vitro* antimicrobial evaluation against clinically relevant drug-resistant strains of methicillin-resistant *Staphylococcus aureus* (MRSA ATCC-43300) and multidrug-resistant *Pseudomonas aeruginosa* (MDR-PA ATCC-27853) showed promising activity: MIC values were 6.25 to 25.0-µg/ml. It is worth highlighting that H2 with 4-methoxyphenyl substituent was more potent (MIC=6.25 µg/ml against MRSA) compared to the standard ciprofloxacin (MIC=16 µg/ml). Assays of crystal violet biofilm inhibition showed concentration-dependent effectiveness of antibiofilm; H2 exhibited 76.4% biofilm reduction at a half of MIC with MRSA. Time-kill kinetics proved the bactericidal effect, and > 4Log$_{10}$ reduction of CFU at 2X MIC. These results set pyrazole-isoxazole hybrids as privileged scaffolds on the formation of subsequent-generation antimicrobials that can interfere with growth of bacteria and resistance by biofilm.

Keywords: hybrids of pyrazole-isoxazole, antimicrobial action, biofilm formation, multidrug resistance, Methicillin-resistant Staphylococcus aureus, Pseudomonas aeruginosa, hydrazone.

INTRODUCTION

Antimicrobial resistance (AMR) is one of the most threatening issues to modern medicine. It is projected that in 2050, 10 million deaths per year could be due to drug-resistant infections, assuming that the current trends would not change (O'Neill, 2016). World Health Organization have been assigned critical priority to Carbapenem-resistant Acinetobacter baumannii, *Pseudomonas aeruginosa*, and *Enterobacteriaceae*, requiring urgent development of novel therapeutic interventions (Tacconelli et al., 2018). In the United States, methicillin resistant *Staphylococcus aureus* (MRSA) alone results in more than 120,000 bloodstream infections annually, and the death rate of the illness is nearly 20 percent, despite the intensive treatment regimens (Kourtis et al., 2019). The pharmacoeconomic impact of MDR infections goes beyond death, including long hospitalization, elevated healthcare expenses that go above 20 billion a year in the U.S., and high productivity loss (Nelson et al., 2021). Gram-negative pathogen like multidrug-resistant *Pseudomonas aeruginosa* is also a unique therapeutic challenge because of intrinsic mechanisms of resistance and lack of effective treatment alternatives (Pang et al., 2019).

The formation of biofilm is an advanced mechanism of bacterial survival. Microorganisms enclose themselves in self-created extracellular polymeric substances (EPS) polysaccharides, proteins, and extracellular DNA (eDNA) creating a 3D structure to endow great resistance to antimicrobial agents. Bacteria in biofilms are evermore 100-1000 times more tolerant than the planktonic counterparts due to low drug penetration into the EPS matrix, metabolic heterogeneity, including dormant persister cells, and horizontal gene transfer of resistance determinants (Hoiby et al., 2010; Stewart and Costerton, 2001). Biofilms are clinically involved in chronic and recurrent infections (80%) such as catheter-associated bloodstream infections, ventilator-associated pneumonia, chronic wound infections, and device-associated infections (Jamal et al., 2018). The resistance character of biofilm infection complex encourages that prolonged high-dose therapy, the frequent removal of the devices, and surgical debridement are used, which are major causes of treatment failure and relapse of the disease (Donlan, 2001). The most recent studies have emphasized the role of quorum sensing (QS) systems as the general controllers of biofilm growth. *LuxS/AI-2* promotes a population density-dependent expression in Gram-negative bacteria, while *agr* systems in *S. aureus*, regulate biofilm maturation and the expression of virulence factors (Papenfort & Bassler, 2016).

Molecular hybridization, which refers to the covalent conjugation of two or more pharmacophoric units with different biological activities into a single molecule, has become an effective approach to drug-design in overcoming multidrug resistance (Meunier, 2008). The following strategic benefits can be achieved by using this strategy: multiple targets on bacteria are engaged at once, which lowers the risk of developing resistance due to the independent mutations; synergistic or additive pharmacological effects can be obtained due to the improved physicochemical properties; and overall potency can be increased (Muregi & Ishih, 2010). Pyrazole derivatives are a privileged scaffold in medicinal chemistry, which has a broad range of biological properties, such as antimicrobial, anti-inflammatory, and anticancer properties (Fustero et al., 2011). The antimicrobial activity of the pyrazoles is also explained by the fact that these compounds can inhibit bacterial DNA gyrase and topoisomerase IV enzymes required in the replication of DNA and survival of bacteria (Osheroff et al., 2026; Collins et al., 2024). The structure-activity relation research has shown that the presence of electron-withdrawing or electron-donating substituents at the 1-position of the pyrazole ring changes the antimicrobial activity via changes in electronic distribution and lipophilicity (Küçükgüzel & Şenkardeş, 2015). Isoxazole heterocycles are also active antimicrobial agents; a number of FDA approved antibiotics including sulfamethoxazole and cloxacillin contain this motif (Zeni 2006). The isoxazole nucleus is also a bioisostere of the carboxylic acids and amides and has a better metabolic stability and good pharmacokinetic characteristics (Khanage et al., 2012). Mechanistic experiments propose that the derivatives of isoxazoles disrupt cell-wall biosynthesis of bacteria and produce antibiofilm effects by interfering with the production of EPS (Bhoye et al., 2025).

Recent medicinal chemistry research has yielded a number of promising heterocyclic antimicrobial products. Pyrazole-thiazole hybrids reported by Gomha et al. (2015) exhibited 4-16 µl/kg MIC values against *MRSA* and E. coli with molecular modeling showing inhibition of DNA gyrase, as the main mode of action. Li et al. (2019) designed quinolone-pyrazole conjugates, which had dual antibacterial and anti-biofilm properties with 65% biofilm inhibition in *P. aeruginosa* at sub-MIC concentrations. Isoxazole compounds containing isoxazole have been particularly

promising to a range of biofilm forming pathogens. Recently, a study by Sofi et al. (2025) described isoxazole derivatives that had dual targeting activity against DNA gyrase and topoisomerase IV, achieving MIC values of 8-32 µg/mL against ESBL-producing *K. pneumoniae*. Schiff base-isoxazole hybrids synthesized by Carreno et al. (2018) showed synergy with colistin against Carbapenem-resistant *A. baumannii*, which is indicative of disruption of the membrane as a contributory mechanism. The Schiff bases that are based on hydrazones have become an effective pharmacophore in the design of antimicrobial drugs. Al-Saleem et al. (2025) have described hydrazone derivatives with high antibacterial activity with a MIC of 4-16 µg/mL on MRSA and other biofilm-inhibitory activity. Hydrazones are characterized by the azomethine (C=N) bond, which gives it conformational flexibility, the ability to form hydrogen-bonds, and possibility of metal-chelation, which helps to maintain its antimicrobial activity (Dongare et al., 2021).

Though these have been made, the evolution of pyrazole isoxazole hybrid scaffolds that are specifically designed to target both planktonic and biofilm embedded drug resistant bacteria has not been well investigated. Previous research has, mostly, examined either antibacterial or antibiofilm activity alone, without systematic analysis of the relationships between structure and activity that control dual functionality. The current study postulate that strategic pyrazole and isoxazole pharmacophores might be incorporated into a single molecular framework by an H2O linkage and this approach will produce dual-action agents that can inhibit vital bacterial enzyme-DNA gyrase and topoisomerase - to produce bactericidal effects on planktonic cultures as well as interfere with bacterial biofilm formation and maturation by disrupting EPS biosynthesis and/or quorum-sensing signaling.

2. MATERIALS AND METHODS

2.1 Chemicals and reagents

The reagents used in this work were purchased at reliable commercial sources (HiMedia, SRL, Sigma-Aldrich) and used in their form, unless it was clearly mentioned that reagent is analytical grade. Reactions were monitored by use of thin - layer chromatography (TLC), with the help of pre-coated silica gel 60 F254 aluminium sheets (Merck). Chromophores were observed with the UV light (254 nm and 365 nm) and /or staining with iodine vapor. The preparative column chromatography was performed using silica gel (100-200 mesh, Merck) and using gradient elution systems as described. The melting points were determined with a Stuart SMP30 apparatus in open capillaries, and uncorrected. ^{1}H-NMR (400 MHz) spectra were recorded on a Bruker Avance III 400 spectrometer using deuterated dimethyl sulfoxide (DMSO-d_6) or chloroform ($CDCl_3$) as solvents, with tetramethylsilane (TMS) as internal standard. Chemical shifts (δ) are reported in parts per million (ppm), and coupling constants (J) in Hertz (Hz). Multiplicities are indicated as: s (singlet), d (doublet), t (triplet), q (quartet), m (multiplet), and br (broad). Fourier-transform infrared (FT-IR) spectra were acquired on a PerkinElmer Spectrum Two spectrometer using KBr pellet technique or attenuated total reflectance (ATR), with absorption bands reported in wavenumbers (cm^{-1}). High-resolution mass spectrometry (HRMS) was performed on a Waters Xevo G2-XS QTof mass spectrometer using electrospray ionization (ESI) in positive ion mode.

2.1.2 Synthesis of Pyrazole-4-carbaldehydes

Synthesis of 1-(4-Chlorophenyl)-1*H*-pyrazole (Intermediate A1):

4-Chlorophenylhydrazine hydrochloride (5.0 g, 27.8 mmol) was dissolved in ethanol (100 mL) in a 250 mL round-bottom flask.

Malondialdehyde bis(diethyl acetal) (6.6 g, 25.0 mmol) and concentrated HCl (5 mL) were added. The resulting mixture was refluxed (78 °C) for 4-6 h with constant stirring. The advancement was followed using TLC (ethyl acetate: hexane 1:4, Rf ~0.5). The reaction mixture was cooled to ambient temperature, poured into ice-water (200 mL) and neutralised to pH-7 using $NaHCO_3$. The product was extracted with dichloromethane (3x 50 mL), dried under the presence of anhydrous Na_2SO_4 and solvent was evaporated using a rotary evaporator. Intermediate A1 was obtained as a white solid (3.9 g, 78%, mp 62-64°C) after column chromatography (silica gel, ethyl acetate:hexane 1:9).

Preparation of 1-(4-Chlorophenyl)-1H-pyrazole-4-carbaldehyde (Intermediate B1):

25 mL DMF was cooled to 0°C in a ice bath. A dropwise addition of $POCl_3$ (2.8 mL, 30 mmol) was done over 15 min (exothermic; temperature kept below 10 °C). A Vilsmeier reagent was formed after 30min stirring. Intermediate A1 (3.5 g, 20 mmol) dissolved in DMF (10 mL) was added, and the mixture was heated up to 80°C (4 h). The mixture was cooled off and transferred into ice-water (200 mL); sodium acetate (20g) was included to hydrolyze it to pH 5 to 6. DCM (3x 50ml) was used to extract the product followed by washing of with water, the product was dried over Na_2SO_4 and the solvent removed. Intermediate B1 was obtained as a pale yellow solid (2.9 g, 70%, mp 112-114°C) by column chromatography (silica gel, ethyl acetate:hexane 1:4).

Synthesis of 1-(4-Methoxyphenyl)-1*H*-pyrazole-4-carbaldehyde (Intermediate B2):

A analogous reaction was made using 4-methoxyphenylhydrazine hydrochloride that resulted in the generation of Intermediate B2 as a pale yellow crystalline product (2.8 g, 72%). mp 108-110°C.

2.1.3 Synthesis of 3-Phenylisoxazole-5-carbohydrazide

Step 1: Synthesis of Benzaldoxime:

Benzaldehyde (5.3g, 50 mmol), and hydroxylamine hydrochloride (3.5g, 50 mmol) were dissolved in ethanol:water (1:1, 50mL). Sodium acetate (4.1 50 mmol) was, then, added, and the mixture stirred for 2h at room temperature. The product was filtered, rinsed with water and dried to obtain benzaldoxime (5.4g, 90%; white solid).

Step 2: Synthesis of Benzohydroximoyl Chloride:

Benzaldoxime (6.0g, 50 mmol) was added to DCM (50mL). N-Chlorosuccinimide (6.7g, 50 mmol) was added portion-wise at 0°C. The solvent was then evaporated after 4h stirring at room temperature, and gave a crude benzohydroximoyl chloride, which was utilized immediately to prevent decomposition.

Step 3: Synthesis of Ethyl 3-Phenylisoxazole-5-carboxylate (Intermediate C):

Crude hydrazoyl chloride was dissolved in ethanol (100mL). Dropwise, ethyl propiolate (4.9 g, 50 mmol) and triethylamine (7 mL, 50 mmol) were added: the mixture was stirred, at room temperature, 12 h. Ethanol was evaporated and water was added and the mixture was extracted using diethyl ether (3 x 50 ml). Intermediate C was purified by column chromatography (silica gel, ethyl acetate:hexane 1:9) followed by a drying over Na_2SO_4 to obtain Intermediate C as a colourless oil (7.6 g, 70% yield).

Step 4: Synthesis of 3-phenylisoxazole- 5-carbohydrazide (Intermediate E):

Intermediate C (4.3g, 20 mmol) was dissolved in ethanol (50 mL). 5ml of hydrazine hydrate (80%, 100mmol) was added and the solution was refluxed over 6h. The precipitate was filtered after

cooling, washed with cold ethanol, and dried to get the Intermediate E as a white solid (3.4 g, 84 %; mp 152-154 °C).

2.1.4 Synthesis of Pyrazole-Isoxazole Hybrids

A mixture of substituted pyrazole-4-carbaldehyde (Intermediate B1 or B2, 10 mmol), 3-phenylisoxazole-5-carbohydrazide (Intermediate E, 10 mmol), and glacial acetic acid (1 mL, catalytic amount) in absolute ethanol (50 mL) was heated under reflux with continuous stirring for 4-6 hours. Reaction progress was monitored by TLC (ethyl acetate:hexane 1:1, product Rf ~0.4). Upon completion, the reaction mixture was cooled to room temperature, and the resulting precipitate was filtered, washed thoroughly with cold ethanol, and dried. The crude product was recrystallized from ethanol to afford pure hybrid compounds.

N'-[(1-(4-Chlorophenyl)-1H-pyrazol-4-yl)methylidene]-3-phenylisoxazole-5-carbohydrazide (H1). Yellowish crystalline solid; Yield: 3.3 g, 85%; mp 206-208°C; ^{1}H-NMR (400 MHz, DMSO-d_6): δ 11.92 (s, 1H, NH), 8.54 (s, 1H, CH=N), 8.42 (s, 1H, H-5 pyrazole), 8.16 (s, 1H, H-3 pyrazole), 7.94 (d, J = 8.8 Hz, 2H, Ar-H ortho to Cl), 7.85-7.82 (m, 2H, Ar-H phenyl), 7.58 (d, J = 8.8 Hz, 2H, Ar-H meta to Cl), 7.51-7.48 (m, 3H, Ar-H phenyl), 7.10 (s, 1H, H-4 isoxazole); FT-IR (KBr, cm^{-1}): 3215 (N-H stretch), 3065 (Ar C-H), 1672 (C=O), 1608 (C=N), 1555, 1485, 1380, 1220, 1080 (C-Cl), 828; ESI-MS m/z: calculated for $C_{20}H_{14}ClN_5O_2$ $[M+H]^+$ 392.0914, found 392.0809.

N'-[(1-(4-Methoxyphenyl)-1H-pyrazol-4-yl)methylidene]-3-phenylisoxazole-5-carbohydrazide (H2). Pale yellow crystalline solid; Yield: 3.2 g, 82%; mp 195-197°C; ^{1}H-NMR (400 MHz, DMSO-d_6): δ 11.85 (s, 1H, NH), 8.50 (s, 1H, CH=N), 8.38 (s, 1H, H-5 pyrazole), 8.12 (s, 1H, H-3 pyrazole), 7.88 (d, J = 9.0 Hz, 2H, Ar-H ortho to OMe), 7.82-7.80 (m, 2H, Ar-H phenyl), 7.48-7.45 (m, 3H, Ar-H phenyl), 7.08 (s, 1H, H-4 isoxazole), 7.02 (d, J = 9.0 Hz, 2H, Ar-H meta to OMe), 3.82 (s, 3H, OCH_3); FT-IR (KBr, cm^{-1}): 3228 (N-H stretch), 3058 (Ar C-H), 2938, 2835 (O-CH_3), 1665 (C=O), 1615 (C=N), 1558, 1512, 1465, 1375, 1248 (C-O), 1025, 835; ESI-MS m/z: calculated for $C_{21}H_{17}N_5O_3$ $[M+H]^+$ 388.1410, found 388.1405.

2.2 Biological Evaluation

2.2.1. Bacterial Strains and Culture Conditions

The antimicrobial efficacy was examined against the clinically relevant multidrug-resistant bacteria including methicillin-resistant *Staphylococcus aureus* (MRSA, ATCC˙43300) and multidrug-resistant *Pseudomonas aeruginosa* (MDR-PA, ATCC 27853). American Type Culture Collection (ATCC) was used to obtain strains. Maintaining of culture was done on Mueller-Hinton agar (MHA) and stored at 4 °C. In the case of experimental inocula, single colonies were transferred into a broth of Mueller-Hinton (MHB) and grown overnight in 37 °C and with the agitation (180 rpm) so that the bacterial culture achieved a mid-logarithmic growth state (OD_{600}=0.4-0.6, which approximates 1-2 x10^8 CFU/mL).

2.2.2 Minimum Inhibitory Concentration (MIC) Determination

96-well Broth microdilution was used to perform MIC assays, according to CLSI (Wayne, 2015). The test compounds were dissolved in DMSO in 5 mg/mL stock solutions. Serial dilutions of 2-fold were made in cation-adjusted Mueller Hinton broth (CAMHB) to produce concentrations of 128 to 0.125 µg/mL. Overnight cultures were diluted with CAMHB to 5 × 10^5 CFU/mL to make bacterial inoculum. Aliquots of 100 µL of each compound dilution were dispensed into wells of a sterile 96-well plate, followed by 100 µL of standardized bacterial suspension. The controls included a positive growth control, sterile medium control, a solvent control

(1% DMSO) and a reference antibiotic (ciprofloxacin). Plates were left to incubate at 37°C for 24h under aerobic conditions. The MIC was determined as the lowest concentration that inhibited the visible growth. Visual assessment was confirmed by measuring optical density at 600 nm (OD_{600}) using a microplate reader (BioTek Synergy H1).

2.2.3 Time-Kill Kinetics Assay

Time-kill using compounds at 1xMIC, 2xMIC and 4xMIC, was performed to explain the phenomenon of bactericidal and bacteriostatic activity against MRSA ATCC 43300. Cultures (10^6 CFU mL^{-1}) were incubated in CAMHB, aliquots (100 µL) were taken at t=0, 2, 4, 6, 8, 12, and 24 h, serially diluted in PBS, and plated on MHA. After incubating the CFUs at 37 °C (24 h), the $\log_{10}$ CFU mL^{-1} values were plotted against time. A reduction of ≥3-$\log_{10}$ relative to the original inoculum at 24 h was considered bactericidal.

2.2.4 Biofilm Formation and Quantification

The assays involving the existence of the static biofilm were conducted using the flat bottomed 96 well polystyrene plates (O'Toole, 2011). Overnight cultures were diluted 1:100 in fresh MHB with 1% glucose. 200 µl Aliquots were dispensed into wells, and incubated at 37°C overnight. PBS washing eliminated non-adherent cells. Biofilms were placed in 99% methanol for 15 minutes followed by the staining with 0.1% crystal violet for 20 minutes at room temperature. The remainder dye was washed out with distilled water; the bound stock was solubilised in 33% of glacial acetic acid and , and absorbance was measured at 570 nm (OD_{570}) using a microplate reader (Stepanović et al., 2007).

2.2.5 Biofilm Inhibition Assay

Bacterial suspensions (10^6 CFU/mL) were pre-inoculated with sub-inhibitory concentrations (1/8× MIC, 1/4× MIC, 1/2× MIC, and 1×MIC) of H1-H2 in order to assess prevention of biofilm formation under inoculation. Biofilms were left to grow in 24 hours and crystal violet staining was done as above. Relative percentage inhibition was determined in comparison to the untreated controls.

2.3 Statistical Analysis

All biological experiments were conducted in triplicate, and data are presented as mean ± standard deviation (SD). Statistical significance was determined using one-way ANOVA with the help of the Tukey's post hoc test for multiple comparisons, *P*-values < 0.001 was taken as significant. GraphPad Prism 9.0 was used to do analyses.

3. RESULTS AND DISCUSSION

3.1 Chemistry and Synthesis

The synthetic plan of pyrazole-isoxazole hybrid compounds is described in Figure 1. Retrosynthetically, the key convergent step was identified as the hydrazone formation of pyrazole-4-carbaldehyde and isoxazole-5-carbohydrazide, enabling structural diversification through variation of substituents on the pyrazole ring. The substituted pyrazoles were formylated in Vilsmeier Haack manner of the respective 1-arylpyrazoles, and the required aldehydes were obtained in 70-72% yields. The 4-chlorophenyl and the 4-methoxyphenyl groups were purposefully selected to test the effect of electron-withdrawing and electron-donating groups on antimicrobial activity. The 3-phenylisoxazole-5-carbohydrazide was prepared in a series of reactions starting with the conversion of the product to an oxime, followed by chlorination, 1,3-dipolarcycloaddition with ethyl propiolate, and the hydrazinolysis reaction with a yield of 53%. The final condensation of the aldehydes to the hydrazide was performed under mild acid catalysis (glacial acetic acid), and the reaction was smooth and provided the target hybrids in high yields (82-85% in ethanol recrystallisation).

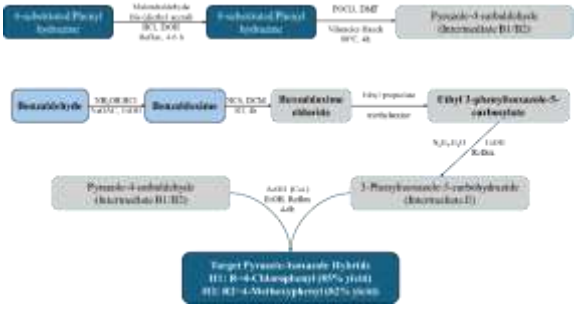

Figure 1: Synthesis of Pyrazole-Isoxazole Hybrids.

Table 1: Physicochemical Properties of Synthesized Pyrazole-Isoxazole Hybrids

Compound	R (Pyrazole substituent)	Molecular Formula	Mol. Weight (g/mol)	Yield (%)	Melting Point (°C)	Log P *
H1	4-Chlorophenyl	$C_{20}H_{14}ClN_5O_2$	391.81	85	206-208	4.18
H2	4-Methoxyphenyl	$C_{21}H_{17}N_5O_3$	387.39	82	195-197	3.92

**Log P values calculated using ChemDraw Professional 20.0.*

A thorough analysis of the structure of compounds H1–H2 was carried out with the help of spectroscopic analysis. The ^{1}H-NMR spectra exhibited typical signals that indicated the formation of hydrazones: the azomethine proton (CH=N) signal was a singlet at δ 8.50-8.54 ppm, the hydrazide NH proton signal was a singlet at δ 11.85-11.92 ppm, and the aromatic protons of the pyrazole, isoxazole and phenyl rings emerged in the corresponding regions (δ 7.02-8.42 ppm). In the case of H2, the methoxy protons were observed as a singlet of δ 3.82ppm. The FT-IR spectroscopy was used to complement the structure; the most notable absorption bands were N-H stretching bands at 3215-3228 cm^{-1}, carbonyl C=O stretching at 1665-1672 cm^{-1}, azomethine C=N stretch at 1608 -1615 cm^{-1}, and aromatic C=C stretch at 1485-1558 cm^{-1}. The absence of aldehyde C=O stretch (usually 1680-1700 cm-1) was indicative of complete conversion to hydrazone product. The molecular ion peaks were confirmed by high-resolution mass spectrometry with acceptable errors, which confirmed the proposed structures and high purity.

3.2 Antimicrobial Activity

The pyrazole-isoxazole hybrids (H1-H2) were tested against a group of clinically significant multidrug resistant bacterial pathogens regarding their antimicrobial activity. **Table-2** provide the observed MIC values, revealing promised activity over Gram-positive (MRSA), and Gram-negative MDR-PA strains.

Table 2: Minimum Inhibitory Concentrations (MIC, µg/mL) of Pyrazole-Isoxazole Hybrids Against Drug-Resistant Bacterial Strains

Compound	MRSA ATCC 43300	MDR-PA ATCC 27853
H1	12.5	25.0
H2	**6.25**	**12.5**
Ciprofloxacin	16.0	64.0

MIC values represent geometric means of three independent experiments performed in triplicate. MRSA: Methicillin-resistant Staphylococcus aureus; MDR-PA: Multidrug-resistant Pseudomonas aeruginosa.

Compound H2 that was 4-methoxyphenyl substituted was been found to have an excellent antimicrobial activity compared to H1 on both the strains examined. H2 showed an MIC of 6.25 µg/mL against MRSA ATCC 43300, which was a 2.5 fold better result compared to the fluoroquinolone standard ciprofloxacin (MIC = 16 µg/mL). This is especially important to note since MRSA strains are often resistant to fluoroquinolone as a result of mutations in DNA gyrase (gyrA) and topoisomerase IV (parC) genes (Hooper & Jacoby 2015). H2 showed an MIC of 12.5 µg/mL against Gram negative MDR *P. aeruginosa* which is a 5-fold stronger than the ciprofloxacin (MIC = 64 µg/mL). Such results are promising, given the inherent resistance mechanisms of *P. aeruginosa*, such as constitutive expression of AmpC β-lactamase, decreased outer membrane permeability, and efflux activity (Pang et al. 2019).

The time-kill kinetics of H2 vs. MRSA ATCC 43300 are represented in Figure-2.

At 1xMIC (6.25µg/mL), H2 caused 2.8 - $\log_{10}$ reduction in viable cell counts after 24h, which is close to the ≥3-$\log_{10}$ decrement threshold of a bactericidal category. Bactericidal activity was further confirmed with 2xMIC (12.5µg/mL) with an 4.2-$\log_{10}$ reduction. Bacterial eradication (>6-$\log_{10}$ reduction, and limit of detection) was attained after 12h at 4xMIC (25 µg/ml). The high-speed kinetics of bactericidal action, especially at high concentrations, suggest that it is directed at the critical bacterial processes. The kill curve versus concentration is consistent with blocking bacterial DNA gyrase or topoisomerase IV -enzymes required in DNA replication and transcription (Drlica & Zhao 1997; Osheroff et al. 2026).

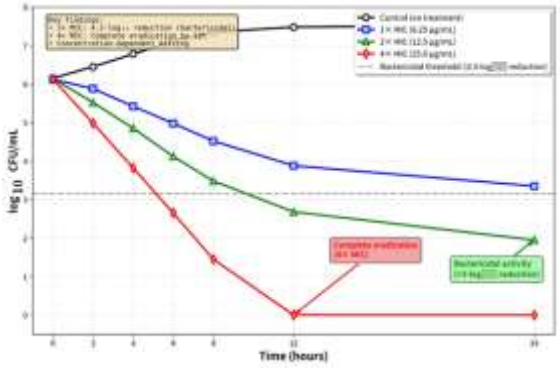

Figure 2: Time kill kinetics of compound H2 against MRSA ATCC 43300.

3.3 Biofilm Studies

Considering the clinical value of biofilm-related infections, the possibility of H1-H2 to inhibit biofilm formation was studied systematically. The two compounds proved to exhibit concentration-dependent biofilm growth inhibition in both the strains examined with H2 performing better than H1 (**Table 3, Figure 3**).

Table 3: Biofilm Inhibition Activity (% Inhibition) of Pyrazole-Isoxazole Hybrids at Sub-MIC Concentrations

Compound	Concentration	MRSA ATCC 43300	MDR-PA ATCC 27853
H1	1/8× MIC	*18.4 ± 2.3*	*12.8 ± 2.8*
	1/4× MIC	*34.6 ± 3.7*	*25.7 ± 3.2*
	1/2× MIC	*58.2 ± 4.1*	*48.3 ± 4.8*
	1× MIC	*82.5 ± 3.2*	*72.9 ± 4.2*
H2	1/8× MIC	*24.8 ± 2.6*	*17.3 ± 3.4*
	1/4× MIC	*45.3 ± 3.4*	*34.8 ± 3.9*
	1/2× MIC	***76.4 ± 3.8***	***63.5 ± 5.1***
	1× MIC	*91.7 ± 2.4*	*81.6 ± 3.6*

Data represent mean ± SD (n = 6). All values significantly different from untreated control (P < 0.001, one-way ANOVA with Tukey's post hoc test).

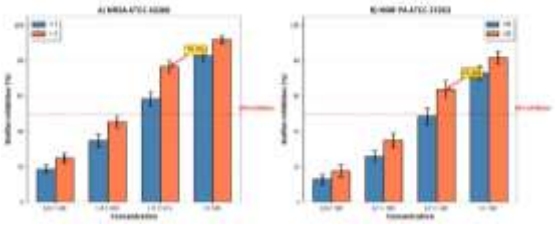

Figure 3: Biofilm inhibition Activity of H1/H2 at sub-MIC concentrations.

It is worth noting that H2 showed 76.4% biofilm inhibition of MRSA at half the MIC (3.125 µg/mL) which was lower than the inhibition of planktonic growth. Clinically, this is a sub-MIC of antibiofilm activity, meaning it is possible to disorient biofilm development without exerting high selective pressure to resist it (Rabin et al. 2015). At the MIC concentration, H2 had more than 90% biofilm inhibitory effect on MRSA, which means that the biofilm architecture was virtually completely prevented. In the case of *P. aeruginosa*, H2 prevented biofilm formation by 63.5% at 0.5xMIC and 81.6% at 1xMIC. The reduced although marginally potency of the Gram negative biofilms could be as a result of variations in the composition of the matrix- *P.aeruginosa* produces polysaccharides (Psl, Pel), extracellular DNA, and proteins that create a hydrated matrix and limit the penetration of the compound (Colvin et al. 2012).

3.4 Structure-Activity Relationship (SAR) Analysis.

The analysis of structural diversity unveils some interesting trends of SAR which can be utilised in future optimisation. The better activity of the H2 (4-methoxyphenyl) compared to the H1 (4-chlorophenyl) indicates that the presence of electron-

giving groups at para-position of the N-aryl substituent increases the antimicrobial and antibiofilm activities. The methoxy group (Hammett σ_para = −0.27) adds density to the electrons of the pyrazole ring by resonance donation, which may enhance the affinity of the methoxy group with bacterial enzyme active sites due to increased π-π stacking and hydrogen-bonding networks. Calculated logP values (H1=4.18, H2=3.92), indicate that both compounds are in the optimum range of antimicrobial activity (logP=3-5), which balances the membrane permeability with aqueous solubility (Lipinski et al. 1997). The slightly reduced logP of H_2 (although with a higher potency) indicates that electronic effects are the main factors to be considered in the strength of this scaffold rather than lipophilicity.

The hydrazone moiety (–C=N–NH–CO–) performs several functions: (i) conformational flexibility that allows it to adapt to many different binding pocket geometries; (ii) an ability to interact via hydrogen-bonds with active-site residues; (iii) a possible ability to chelate metals to inhibit metalloenzymes; and (iv) metabolically not readily hydrolyzed by enzymes as compared to esters or amides (Narang et al. 2012). The future analogs should therefore consider additional electron donating groups to the pyrazole N-aryl ring (-CH_3, -$N(CH_3)_2$, -OH), other types of heterocyclic replacements to the phenyl rings (pyridyl, thienyl), and to regioisomeric patterns of pyrazole 3-phenyl ring substitution.

3.5 Postulated Dual Action Mechanism

A combination of the data of antimicrobial and antibiofilm and time-kill provides a mechanistic model of the dual action of pyrazole-isoxazole hybrids. Against planktonic bacteria, it is likely to act through: (1) penetration through bacterial membrane by optimum lipophilicity (logP 6 -4); (2) accumulation in the cell so as to access the essential enzymes; (3) binding to DNA gyrase/topoisomerase IV active sites, therefore, inhibiting DNA supercoiling; (4) as a result, disruption of DNA replication and transcription; and (5) bactericidal cell death as demonstrated by >3-$\log_{10}$ decreases in time -kill This is consistent with the approved antimicrobial target type II topoisomerases (Osheroff et al. 2026; Collins et al. 2024).

It is likely that the antibiofilm activity is based on: (1) penetration through the extracellular polymeric substance matrix, supported by moderate lipophilicity; (2) interference with matrix biosynthesis via inhibition of EPS producing enzymes; (3) potential interference with quorum -sensing signalling; (4) combined bactericidal action on embedded bacteria; and (5) overall destabilization of biofilm structure, as shown by reduction of biofilm by more than 70 per cent at sub-MIC. The sub-MIC antibiofilm effect suggests that it is targeting biofilm-specific pathways that are independent of key metabolic functions and thus reducing the selection pressure against resistance.

CONCLUSION

This study confirms pyrazole-isoxazole hybrids as an emerging and potentially effective fifth generation dual-activity antimicrobial agent meeting a serious unmet gap in therapy of both the planktonic and biofilm-embedded drug-resistant bacterial populations. H2, the lead compound, has a strong broad-spectrum antibacterial effect (MIC = 6.25 to 12.5µg/ml) against MRSA and MDR *P. aureus*, which was 2.5 to 5 times potent than ciprofloxacin. Superior antibiofilm activity was noted with 76.4% inhibition of MRSA at 1/2 MIC and above 90% at 1/MIC. The demonstration of a bactericidal reaction by time-kill kinetics with >4-$\log_{10}$ reductions at 2X MIC in 24 hours was compatible with a target engagement of DNA gyrase/topoisomerase IV. Positive SAR demonstrated that positive SAR effects of electron-donating substituents (4-

methoxy> 4-chloro) can be observed to improve antimicrobial and antibiofilm activities and the logP values (3.92-4.18) belong to drug-likeness window. The suggested dual targeting approach, which is DNA replication inhibition and biofilm matrix disruption, is a powerful concept to reduce the emergence of resistance.

The dual-action profile of the pyrazole-isoxazole hybrids is to take care of several aspects of antimicrobial resistance. These compounds may be promising in chronic infection environments where biofilms promote treatment failure, including catheter-associated infections, chronic wounds, and osteomyelitis by inhibiting biofilm formation at lower (sub-MIC) concentrations. The DNA replication and biofilm formation are targeted simultaneously decreasing the chances of developing resistance through independent mutations, and potentially prolonging a therapeutic lifespan. Both Gram-positive MRSA and Gram-negative MDR-PA priority pathogens are positioned as candidate empirical treatments of polymicrobial infections.

These encouraging results are, however, limited in a number of ways. This experiment was done with just two analogues, a complete SAR search with diverse electronic, steric, and lipophilic analogues is needed to establish the ideal pharmacophores. *In vitro* tests are not sufficient to determine *in vivo* efficacy and thus animal infection models (murine thigh infection model, catheter biofilm models) and PK/PD are essential. The ADME properties, including oral bioavailability, tissue distribution, metabolic stability, and clearance are not characterized. The therapeutic index needs to be determined by cytotoxicity and haemolysis tests. Molecular docking and enzymatic experiments (DNA gyrase IC_{50}, topoisomerase IV IC_{50}) will validate the suggested mechanism and discover particular targets.

Future research directions must focus on: synthesis of 20-30 analogues with diversified pyrazole and isoxazole substituents to optimise potency and selectivity; *in vivo* efficacy studies in germane infection models with PK/PD profiling; detailed ADME/toxicology analysis including oral bioavailability, tissue distribution, cytotoxicity, and genotoxicity; mechanistic validation of activity by the use of enzymatic assays, thermal shift assays, and resistance profiling by serial passage; and formulation development to include solubility improvement and stability. The pyrazole-isoxazole hybrids presented in the present paper demonstrate that careful molecular engineering, based on the principles of medicinal-chemistry, could result in dual-action agents that would address several levels of antimicrobial resistance. Their in-vitro profile, which consists of high antimicrobial efficacy, high antibiofilm efficacy, and a bactericidal mechanism, should be further explored to be developed into clinical applications to supplement the therapeutic capabilities of the current available therapeutic tools against biofilm-forming multidrug-resistant bacterial pathogens.

Conflict of Interest

The authors declare no competing financial interests or conflicts of interest related to this work.

References

Al-Saleem, M. S., Mohamed Ahmed, M. S., Riyadh, S. M., Alruwaili, A. H., Zaki, M. E., & Gomha, S. M. (2025). Synthesis, Molecular Characterization, and Antimicrobial Evaluation of Hydrazones Derived from 2-Hydrazinobenzimidazole. *Drug Design, Development and Therapy*, 4437-4456.

Bhoye, M. R., Shinde, A., Shaikh, A. L. N., Shisode, V., Chavan, A., Maliwal, D., ... & Mhaske, P. C. (2025). New thiazolyl-isoxazole derivatives as potential anti-

infective agents: design, synthesis, in vitro and in silico antimicrobial efficacy. *Journal of Biomolecular Structure and Dynamics*, *43*(10), 5053-5067.

Carreño, A., Zúñiga, C., Páez-Hernández, D., Gacitúa, M., Polanco, R., Otero, C., ... & Fuentes, J. A. (2018). Study of the structure–bioactivity relationship of three new pyridine Schiff bases: synthesis, spectral characterization, DFT calculations and biological assays. *New Journal of Chemistry*, *42*(11), 8851-8863.

Collins, J. A., & Osheroff, N. (2024). Gyrase and topoisomerase IV: recycling old targets for new antibacterials to combat fluoroquinolone resistance. *ACS infectious diseases*, *10*(4), 1097-1115.

Colvin, K. M., Irie, Y., Tart, C. S., Urbano, R., Whitney, J. C., Ryder, C., ... & Parsek, M. R. (2012). The Pel and Psl polysaccharides provide Pseudomonas aeruginosa structural redundancy within the biofilm matrix. *Environmental microbiology*, *14*(8), 1913-1928.

Dongare, G., & Aswar, A. (2021). Synthesis, spectral characterization, thermo-kinetic and biological studies of some complexes derived from tridentate hydrazone Schiff base. *Journal of Saudi Chemical Society*, *25*(10), 101325.

Donlan, R. M. (2001). Biofilm formation: a clinically relevant microbiological process. *Clinical infectious diseases*, *33*(8), 1387-1392.

Drlica, K., & Zhao, X. (1997). DNA gyrase, topoisomerase IV, and the 4-quinolones. *Microbiology and molecular biology reviews*, *61*(3), 377-392.

Flemming, H. C., & Wingender, J. (2010). The biofilm matrix. *Nature reviews microbiology*, *8*(9), 623-633.

Fustero, S., Sánchez-Roselló, M., Barrio, P., & Simon-Fuentes, A. (2011). From 2000 to mid-2010: A fruitful decade for the synthesis of pyrazoles. *Chemical reviews*, *111*(11), 6984-7034.

Gomha, S. M., Riyadh, S. M., Mahmmoud, E. A., & Elaasser, M. M. (2015). Synthesis and anticancer activities of thiazoles, 1, 3-thiazines, and thiazolidine using chitosan-grafted-poly (vinylpyridine) as basic catalyst. *Heterocycles*, *91*(6), 1227-1243.

Høiby, N., Bjarnsholt, T., Givskov, M., Molin, S., & Ciofu, O. (2010). Antibiotic resistance of bacterial biofilms. *International journal of antimicrobial agents*, *35*(4), 322-332.

Hooper, D. C., & Jacoby, G. A. (2015). Mechanisms of drug resistance: quinolone resistance. *Annals of the New York academy of sciences*, *1354*(1), 12-31.

Jamal, M., Ahmad, W., Andleeb, S., Jalil, F., Imran, M., Nawaz, M. A., ... & Kamil, M. A. (2018). Bacterial biofilm and associated infections. *Journal of the chinese medical association*, *81*(1), 7-11.

Khanage, S., Mohite, P., Pandhare, R., & Raju, A. (2012). Synthesis and pharmacological evaluation of isoxazole derivatives containing 1, 2, 4-triazole Moiety. *Marmara pharmaceutical Journal*, *16*(2), 134-140.

Kourtis, A. P., Hatfield, K., Baggs, J., Mu, Y., See, I., Epson, E., ... & Ray, S. M. Emerging Infections Program MRSA author group, Ham D, Capers C, Ewing H, Coffin N, McDonald LC, Jernigan J, Cardo D. 2019. *Vital signs: epidemiology and recent trends in methicillin-resistant and in methicillin-susceptible Staphylococcus aureus bloodstream infections—United States. MMWR Morb Mortal Wkly Rep*, *68*, 214-219.

Küçükgüzel, Ş. G., & Şenkardeş, S. (2015). Recent advances in bioactive pyrazoles. *European Journal of Medicinal Chemistry*, *97*, 786-815.

Li, S., Hu, L., Li, J., Zhu, J., Zeng, F., Huang, Q., ... & Cao, R. (2019). Design,

synthesis, structure-activity relationships and mechanism of action of new quinoline derivatives as potential antitumor agents. *European Journal of Medicinal Chemistry*, *162*, 666-678.

Lipinski, C. A., Lombardo, F., Dominy, B. W., & Feeney, P. J. (1997). Experimental and computational approaches to estimate solubility and permeability in drug discovery and development settings. *Advanced drug delivery reviews*, *23*(1-3), 3-25.

Meunier, B. (2008). Hybrid molecules with a dual mode of action: dream or reality?. *Accounts of chemical research*, *41*(1), 69-77.

Muregi, F. W., & Ishih, A. (2010). Next-generation antimalarial drugs: hybrid molecules as a new strategy in drug design. *Drug development research*, *71*(1), 20-32.

Narang, R., Narasimhan, B., & Sharma, S. (2012). A review on biological activities and chemical synthesis of hydrazide derivatives. *Current medicinal chemistry*, *19*(4), 569-612.

Nelson, R. E., Hatfield, K. M., Wolford, H., Samore, M. H., Scott, R. D., Reddy, S. C., ... & Baggs, J. (2021). National estimates of healthcare costs associated with multidrug-resistant bacterial infections among hospitalized patients in the United States. *Clinical Infectious Diseases*, *72*(Supplement_1), S17-S26.

O'Neill, J. (2016). *Tackling drug-resistant infections globally: Final report and recommendations*. Review on Antimicrobial Resistance.

Osheroff, N. (2026). Gyrase and Topoisomerase IV as Antibacterial Targets for Gepotidacin and Zoliflodacin: Teaching Old Enzymes New Tricks. *International Journal of Molecular Sciences*, *27*(1), 496.

O'Toole, G. A. (2011). Microtiter dish biofilm formation assay. *Journal of Visualized Experiments*, (47), e2437.

Pang, Z., Raudonis, R., Glick, B. R., Lin, T. J., & Cheng, Z. (2019). Antibiotic resistance in Pseudomonas aeruginosa: mechanisms and alternative therapeutic strategies. *Biotechnology advances*, *37*(1), 177-192.

Pankey, G. A., & Sabath, L. D. (2004). Clinical relevance of bacteriostatic versus bactericidal mechanisms of action in the treatment of Gram-positive bacterial infections. *Clinical infectious diseases*, *38*(6), 864-870.

Papenfort, K., & Bassler, B. L. (2016). Quorum sensing signal–response systems in Gram-negative bacteria. *Nature Reviews Microbiology*, *14*(9), 576-588.

Rabin, N., Zheng, Y., Opoku-Temeng, C., Du, Y., Bonsu, E., & Sintim, H. O. (2015). Biofilm formation mechanisms and targets for developing antibiofilm agents. *Future medicinal chemistry*, *7*(4), 493-512.

Sofi, F. A., Masoodi, M. H., & Tabassum, N. (2025). Recent advancements in the development of next-generation dual-targeting antibacterial agents. *RSC Medicinal Chemistry*, *16*, 1891-1922.

Stepanović, S., Vuković, D., Hola, V., Bonaventura, G. D., Djukić, S., Ćirković, I., & Ruzicka, F. (2007). Quantification of biofilm in microtiter plates: overview of testing conditions and practical recommendations for assessment of biofilm production by staphylococci. *Apmis*, *115*(8), 891-899.

Stewart, P. S., & Costerton, J. W. (2001). Antibiotic resistance of bacteria in biofilms. *The lancet*, *358*(9276), 135-138.

Tacconelli, E., Carrara, E., Savoldi, A., Harbarth, S., Mendelson, M., Monnet, D. L., ... & Zorzet, A. (2018). Discovery, research, and development of new antibiotics: the WHO priority list of

antibiotic-resistant bacteria and tuberculosis. *The Lancet infectious diseases*, *18*(3), 318-327.

Wayne, P. A. (2015). Clinical and laboratory standards institute (CLSI). *Performance standards for antimicrobial susceptibility testing*, *30*.

Zeni, G., & Larock, R. C. (2006). Synthesis of heterocycles via palladium-catalyzed oxidative addition. *Chemical reviews*, *106*(11), 4644-4680.